

Optimal Motion Planning for Quadruped Manipulators in Heavy Payload Transportation Tasks

Ioannis Dadiotis, Arturo Laurenzi and Nikos Tsagarakis

Abstract—This work presents a simplified model-based trajectory optimization (TO) formulation for planning motions on quadruped mobile manipulators that locomote while carrying heavy payload. The formulation considers both robot and payload dynamics and simultaneously plans locomotion and payload manipulation trajectories. Thanks to the heavy payload manipulation planning the resulted payload-aware planner is less prone to leg singular configurations in kinematically demanding motions compared to its locomotion-only counterpart. The method is validated on the quadruped bi-manual CENTAURO robot carrying a payload that consists 85 % of the arms' payload capacity and exceeds 15 % of the robot's mass.

Paper Type – Recent Work [1] (under review)

I. MOTIVATION

Great progress in motion planning and control of legged robots has enabled deployment of quadruped platforms for mapping and exploration of real-world environments [2]. Despite this achievement, the use of quadruped robots in a wider range of tasks like mobile manipulation remains an open challenge. In contrast to aerial robots, quadruped manipulators are more promising for all-terrain applications that require executing manipulation actions with large physical interaction due to the legged contact and articulation. This promise has in no case been fulfilled so far since very few works [3]–[9] have addressed the problem of simultaneously performing locomotion and manipulation tasks on real quadruped manipulators. Among them, only [8], [9] optimize locomotion and manipulation motions concurrently in the planning stage.

Among other challenging tasks, quadruped manipulators promise robotizing heavy payload transportation in non-flat terrain. This task poses significant challenges to the robot, namely compromising stability, forcing actuator saturation and reaching joint limits. As a result, despite the existence of numerous quadruped manipulators [3]–[5], [10]–[13], their deployment and feasibility to maintain locomotion while carrying heavy payload (more than 15 % of the robot's mass) has been either relatively unexplored or compromised by generating motions only for the lower body of the robot [14]. This work introduces a model-based TO formulation that optimizes locomotion, manipulation and payload dynamics. The proposed framework is validated on the quadruped bi-manual CENTAURO robot while carrying 17 kg payload, as shown in Fig. 1.

All co-authors are with Humanoid and Human-Centered Mechatronics Research Line, Italian Institute of Technology, Genoa 16163, Italy (emails: name.surname@iit.it). I.D. is also with the Department of Informatics, Bioengineering, Robotics and Systems Engineering, University of Genoa, Genoa 16145, Italy.



Fig. 1. The CENTAURO robot walking while carrying 17 kg payload.

II. TRAJECTORY OPTIMIZATION FORMULATION

The TO framework is formulated by transcribing the continuous optimization problem in a constrained Nonlinear Programming (NLP) problem with a finite set of decision variables. The formulation plans both locomotion and manipulation trajectories for the task of carrying heavy payload with known mass¹. Henceforth, the TO framework is referred as *payload-aware planner*. The formulation optimizes the CoM state $\mathbf{z}(t) = [\mathbf{r}(t) \ \dot{\mathbf{r}}(t) \ \ddot{\mathbf{r}}(t)]^T$ (where $\mathbf{r}(t)$ is the CoM position), the CoM jerk, the motion of the arm EEs as well as the forces $\mathbf{f}_i(t)$ at all (feet and arm) EEs for the desired stride (i.e. feet EE trajectories are defined by the user). The CoM position is parameterized as cubic spline, the EE forces as piecewise linear while Cubic Hermite Parameterization (CHP) [15] is used for the arm EEs position.

A. The robot model

The robot is modeled using the Single Rigid Body Dynamics (SRBD) model with point contacts. The SRBD model is described by the following equation:

$$\begin{bmatrix} \dot{\mathbf{P}} \\ \dot{\mathbf{L}} \end{bmatrix} = \begin{bmatrix} m\mathbf{g} + \sum_{i=1}^{n_{cont}} \mathbf{f}_i \\ \sum_{i=1}^{n_{cont}} (\mathbf{p}_i - \mathbf{r}) \times \mathbf{f}_i \end{bmatrix} \quad (1)$$

where $\dot{\mathbf{P}} = m \cdot \dot{\mathbf{r}}$ and $\dot{\mathbf{L}}$ are the derivatives of the linear and angular momentum, respectively, \mathbf{g} is the gravity vector, \mathbf{p}_i denotes the feet EE position vectors, m is the robot mass and the number of contacts $n_{cont} = 6$ (since both feet and arm EEs can make contact with the environment). Since base

¹The mass of a grasped payload can be estimated through force estimation at the EE using a wrist force/torque sensor or by exploring the joint torque sensing available on the arm.

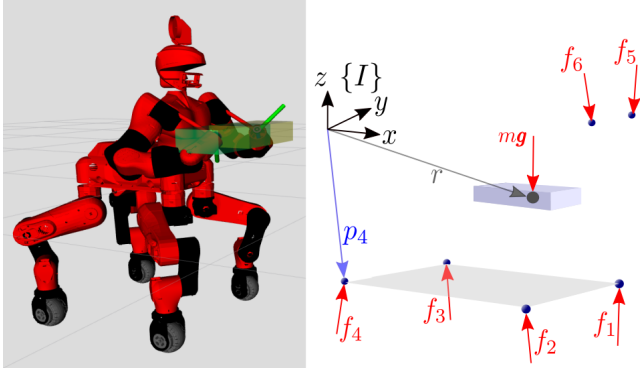


Fig. 2. Visualization of the CENTAURO robot with the arm EE box workspaces (left). The simplified dynamic model considered by the payload-aware planner (right). For the sake of clarity, the position vector \mathbf{p}_i with respect to (wrt) the inertial frame I is depicted for one EE.

angular motion is not optimized, constant angular momentum is, further, assumed $\dot{\mathbf{L}} = \mathbf{0}$. In the following section it is discussed how the formulation is made robust against the significant assumptions of the SRBD model.

B. Locomotion-related behavior

The CoM state and its derivative are related with the CoM jerk through an equality constraint that describes a triple integrator system. The unilateral and friction pyramid constraints are imposed for the feet in contact as inequality constraints. To compensate for the assumptions of the SRBD model (e.g. massless limb assumption), large stability bounds are imposed by setting a positive lower bound for the normal component of the force at each foot in contact. Finally, the initial CoM state, \mathbf{z}_0 is enforced while the final CoM position is bounded within a desired region (centered around the nominal CoM position on the final footholds). Final CoM velocity and acceleration are bounded to zero.

CoM jerk and feet EE force components \mathbf{f}_i^{xy} are penalized in order to avoid oscillatory trajectories and favor forces close to contact normals, respectively. Finally, a penalty cost is included for the CoM position with the form:

$$J_r = \|\mathbf{r} - (\mathbf{p}_{mean} + \mathbf{c}_{ref})\|^2 \quad (2)$$

where $\mathbf{p}_{mean} = \frac{1}{n_{cont}} \sum_{i=1}^{n_{cont}} \mathbf{p}_i$ is the mean of the feet EE position vectors (regardless of contact state) and \mathbf{c}_{ref} is a robot-specific vector with only vertical component (so that the CoM reference point is above \mathbf{p}_{mean}). This way motions with the CoM horizontal projection close to the geometric center of the feet EE formed polygon are favored.

C. Payload manipulation-related behavior

Under the presence of payload, the robot arms are in continuous contact with the payload, therefore, the motion of each payload is identical to the motion of the arm EE that carries it. The motion planner accounts for each grasped payload dynamics by considering a point mass model with the following equality constraint:

$$m_{pay} \cdot \ddot{\mathbf{p}}_{pay} = m_{pay} \cdot \mathbf{g} + \mathbf{f}_{pay,i} \quad (3)$$

where $\ddot{\mathbf{p}}_{pay} = \ddot{\mathbf{p}}_i$ is the payload acceleration (identical to the arm EE's), m_{pay} is the payload mass and $\mathbf{f}_{pay,i} = -\mathbf{f}_i$ is the force exerted to the payload (equal and opposite to the arm EE force). Subscript $i \in \{5, 6\}$ refers to the arm EEs.

The arm EE trajectories are constrained to remain within boxes (shown in Fig. 2) that are centered at the nominal position wrt the CoM $\bar{\mathbf{p}}_{ri}$ and aligned with the inertial frame. This inequality constraint for each arm EE is described as:

$$|(\mathbf{p}_i - \mathbf{r} - \bar{\mathbf{p}}_{ri})^T \hat{\mathbf{j}}| \leq 0.5 \cdot \mathbf{b}_{ee}^T \hat{\mathbf{j}} \quad (4)$$

where $\hat{\mathbf{j}} \in \{\hat{\mathbf{x}}, \hat{\mathbf{y}}, \hat{\mathbf{z}}\}$ are the unit vectors along the inertial directions and \mathbf{b}_{ee} is a 1×3 array matrix including the box dimensions. The two workspaces are selected to overlap with each other in order to provide the solver with more freedom and self-collision avoidance is ensured with another constraint that requires the distance between the two EEs along the y inertial direction to be greater than a safety threshold.

Initial position, zero initial and final velocity of the arm EEs are enforced while a constraint for arm EE CHP acceleration equality at polynomial junctions is included.

Finally, the magnitude of each arm EE force is bounded with a box constraint, which results in bounding the corresponding arm EE acceleration. This is because each arm EE and the corresponding payload are subject to the same acceleration, which is coupled with the force at the arm EE through the payload dynamics (3). Each arm EE force box is centered at the payload's weight vector $m_{pay} \cdot \mathbf{g}$, thus the constraint has the form:

$$|(\mathbf{f}_i - m_{pay} \cdot \mathbf{g})^T \hat{\mathbf{j}}| \leq 0.5 \cdot \mathbf{b}_f^T \hat{\mathbf{j}} \quad (5)$$

where \mathbf{b}_f is a 1×3 array matrix including the box dimensions. The larger the bounding boxes are, the more dynamic arm motions the framework is permitted to plan.

For each arm a cost is added to favor motions with small EE acceleration (among the ones specified through (5)). This cost has analytical form and penalizes the integral of the squared acceleration polynomial. The latter can be reconstructed from the acceleration at the knots based on the selected parameterization and, thus, is available to the planner. The analytical cost penalizes acceleration through the whole spline and not just at the knots.

III. WHOLE-BODY CONTROLLER (WBC)

The CoM and EE position trajectories are fed to a WBC that is based on hierarchical optimization and inverse kinematics (IK). The WBC is developed within the framework of [16] and is responsible for generating the motions for all the robot joints. Joint trajectories are then fed to the low-level joint position controllers. The structure of the WBC (stack of tasks) is shown in Table I. It is worth mentioning that sufficient control authority is assumed and joint torque limits are not considered, which can be a limitation for very dynamic motions.

TABLE I
WBC TASKS AND CONSTRAINTS

| Priority | Tasks |
|------------|------------------------|
| 1 | Feet position tracking |
| 1 | CoM position tracking |
| 2 | Arms position tracking |
| 3 | Postural task |
| Constraint | Joint position limits |
| Constraint | Joint velocity limits |

IV. RESULTS

The framework is tested in a variety of simulation and experimental scenarios and compared with its locomotion-only counterpart. The latter is derived by excluding any manipulation-related quantity (decision variables, constraints, costs) referred in Sec. II, considering payload as part of the robot model and generate motion only for the joints of the robot's lower body.

A. Kinematically demanding motions

Under heavy payload, large CoM motions may be necessitated in order to compensate for the payload effect. In kinematically demanding motions, e.g. large strides where swing distance is large, swing leg may be outstretched and reach its workspace kinematic limit, a configuration known as *boundary singularity*. The manipulability metric (6) is used to evaluate the distance of a leg configuration from singularity.

$$w(\mathbf{q}) = \sqrt{\det(\mathbf{J}_u(\mathbf{q})\mathbf{J}_u^T(\mathbf{q}))} \quad (6)$$

where \mathbf{J}_u is the linear velocity jacobian of the foot EE wrt the base link while the joint position vector \mathbf{q} is computed by the WBC. Due to the optimization of the payload manipulation in the NLP formulation and, consequently, the deployment of the robot's upper body the payload-aware planner leads to higher, compared with the locomotion-only case, feet EEs manipulability.

In Fig. 3 snapshots of a lateral stepping experiment with 8.5 kg payload at each arm (85 % of the arm's payload capacity, total 15.1 % of the robot mass) are shown. The generated trajectories are accurately tracked from the real hardware such that the real FR leg manipulability remains higher than the one planned in the locomotion-only case.

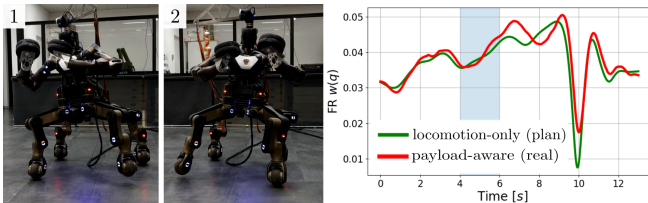


Fig. 3. Snapshots of lateral walking experiments on flat terrain (left) and FR leg manipulability comparison based on experimental and simulation data on the payload-aware and locomotion-only cases, respectively. (right)

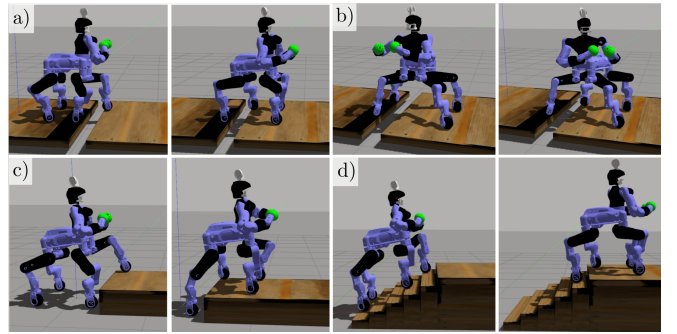


Fig. 4. CENTAURO negotiating non-flat terrain while carrying 20 kg payload in simulation. a) 0.2 m gap, b) 0.25 m gap, c) 0.3 m height platform and d) staircase. Motion plans from consecutive TOs with 4 step horizon are replayed. The attached green ball EEs consist the attached payloads.

B. Non-flat terrain

Larger motions are synthesized by running TO with 4 step horizon and replaying them consecutively on the robot. Using the presented planner CENTAURO is shown to negotiate gaps, a 0.3 m height platform (36.8 % of leg's length) and a staircase in simulation, as shown in Fig. 4.

On real hardware, stepping up on a 0.3 m height platform (through multiple offline TOs), is shown in Fig. 5². The wheeled capabilities of the robot are not used in order to stress the efficiency of the proposed framework. It is noted that the used boxes in (4) are set more conservative than in simulation due to the larger size of the real attached payload. Moreover, a larger stability bound (mentioned in Sec. II-B) is used to increase robustness against modelling inaccuracies between the simulated and real robot model.

In Fig. 5 the planned and estimated normal to the contact plane force components during the platform stepping up experiment are depicted for the feet EEs. The estimated forces follow in general the trend of the planned ones. The presented force tracking errors are mainly due to the fact that forces are not explicitly tracked, joint position control is used (there is force redundancy) and there are estimation errors. Finally, the estimated force components in Fig. 5 often reach low values at each leg when the one diagonal to it is swinging due to the momentum produced by the joint velocities when swinging fast a robot leg.

C. Computational efficiency

In Table II (OFF row) the computational load of the introduced framework is presented for planning three different motion scenarios: 4 steps of 0.25 m along the longitudinal robot direction on flat terrain (a single TO with 13 sec. horizon), 4 steps of 0.25 m along the lateral robot direction on flat terrain (a single TO with 13 sec. horizon) and the step-up motion of Fig. 4c (multiple replayed TOs with total duration 46 sec.). The time needed for the optimal solution is more than 30 times shorter than the planning horizon, namely ~ 400 ms for 13 sec. and ~ 1.4 s for 46 sec. of motion,

²The video of the experiment is included in the accompanying video which is also available in <https://youtu.be/gzm46wSfWAI>.

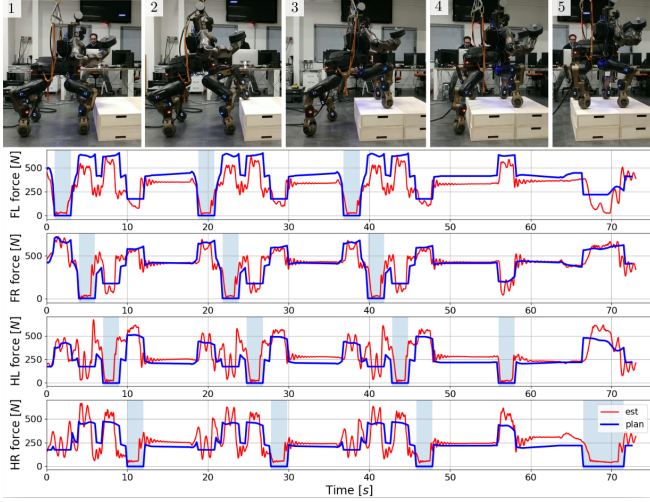


Fig. 5. Snapshots of CENTAURO stepping up on a 0.3 m height platform (top), planned (blue) and estimated (red) normal force component at feet EEs (bottom). Shaded regions denote swing periods.

respectively. The above mean values were calculated from 5 samples. Zero initial guess was provided to the solver.

Based on the achieved performance the formulation can, also, run in a receding horizon fashion. Continuous walking with the strides of Table II and the step up motion is planned online at 5 Hz with 4 sec. horizon. The implementation provides insight about the potentiality of the approach for online planning. Initial guess consisted of the previous solution for the common knots and the last available knot solution for the remaining knots is provided. The mean convergence time for a solution, calculated from multiple trials, is shown in Table II (RH row). Although the horizon is of considerable length convergence time is more than 50 times shorter (75 times for the step up motion), which renders future implementations of higher planning frequency and NLP resolution feasible.

TABLE II

PAYOUT-AWARE OFFLINE (OFF) AND RECEDING HORIZON (RH) - MEAN CONVERGENCE TIME (ITERATIONS)

| | Longitudinal [ms] | Lateral [ms] | Step up [s] |
|-----|-------------------|--------------|-------------|
| OFF | 375.34 (44) | 399.44 (46) | 1.41 (194) |
| RH | 60.43 (15) | 64.53 (16) | 0.053 (13) |

V. CONCLUSION

We present results of a model-based TO formulation on the quadruped bi-manual CENTAURO robot for heavy payload transportation tasks. The proposed framework co-optimizes locomotion and payload manipulation and is combined with an IK-based WBC. The framework demonstrates efficiency on flat and non-flat terrain under payload that exceeds 15 % of the robot's mass and overcomes its locomotion-only counterpart which can be poor for kinematically demanding motions. The presented formulation can be, as well, used for online receding horizon planning.

REFERENCES

- I. Dadiotis, A. Laurenzi, and N. Tsagarakis, "Trajectory optimization for quadruped mobile manipulators that carry heavy payload," in *2022 IEEE/RSJ International Conference on Intelligent Robots and Systems (IROS)*. IEEE, 2022 (submitted).
- M. Tranzatto, F. Mascalich, L. Bernreiter, C. Godinho, M. Camurri *et al.*, "Cerberus: Autonomous legged and aerial robotic exploration in the tunnel and urban circuits of the darpa subterranean challenge," 2022. [Online]. Available: <https://arxiv.org/abs/2201.07067>
- C. D. Bellicoso, K. Krämer, M. Stäuble, D. Sako, F. Jenelten *et al.*, "Alma-articulated locomotion and manipulation for a torque-controllable robot," in *2019 International Conference on Robotics and Automation (ICRA)*. IEEE, 2019, pp. 8477–8483.
- S. Zimmermann, R. Poranne, and S. Coros, "Go fetch! - dynamic grasps using boston dynamics spot with external robotic arm," in *2021 IEEE International Conference on Robotics and Automation (ICRA)*. IEEE, 2021.
- "Boston dynamics: Spot's got an arm!" <https://youtu.be/6Zbhvaac68Y>, accessed: 2021-02-25.
- M. P. Murphy, B. Stephens, Y. Abe, and A. A. Rizzi, "High degree-of-freedom dynamic manipulation," in *Unmanned Systems Technology XIV*, vol. 8387. International Society for Optics and Photonics, 2012, p. 83870V.
- Y. Ma, F. Farshidian, T. Miki, J. Lee, and M. Hutter, "Combining learning-based locomotion policy with model-based manipulation for legged mobile manipulators," *IEEE Robotics and Automation Letters*, vol. 7, no. 2, pp. 2377–2384, 2022.
- J.-P. Sleiman, F. Farshidian, M. V. Minniti, and M. Hutter, "A unified mpc framework for whole-body dynamic locomotion and manipulation," *IEEE Robotics and Automation Letters*, vol. 6, no. 3, pp. 4688–4695, 2021.
- J.-R. Chiu, J.-P. Sleiman, M. Mittal, F. Farshidian, and M. Hutter, "A collision-free mpc for whole-body dynamic locomotion and manipulation," 2022.
- B. U. Rehman, D. G. Caldwell, and C. Semini, "Centaur robots-a survey," in *Human-Centric Robotics: Proceedings of CLAWAR 2017: 20th International Conference on Climbing and Walking Robots and the Support Technologies for Mobile Machines*. World Scientific, 2018, pp. 247–258.
- N. Kashiri, L. Baccelliere, L. Muratore, A. Laurenzi, Z. Ren *et al.*, "Centauro: A hybrid locomotion and high power resilient manipulation platform," *IEEE Robotics and Automation Letters*, vol. 4, no. 2, pp. 1595–1602, 2019.
- "It: Robot teleoperativo," <https://youtu.be/66ZMUaBLJaM>, accessed: 2021-02-25.
- "Boston dynamics: Dynamic robot manipulation," <https://youtu.be/2jvLalY6ubc>, accessed: 2021-02-25.
- X. Zhao, Y. You, A. Laurenzi, N. Kashiri, and N. Tsagarakis, "Locomotion adaptation in heavy payload transportation tasks with the quadruped robot centauro," in *2021 IEEE International Conference on Robotics and Automation (ICRA)*. IEEE, 2021.
- A. W. Winkler, C. D. Bellicoso, M. Hutter, and J. Buchli, "Gait and trajectory optimization for legged systems through phase-based end-effector parameterization," *IEEE Robotics and Automation Letters*, vol. 3, no. 3, pp. 1560–1567, 2018.
- E. M. Hoffman, A. Rocchi, A. Laurenzi, and N. G. Tsagarakis, "Robot control for dummies: Insights and examples using opensot," in *2017 IEEE-RAS 17th International Conference on Humanoid Robotics (Humanoids)*. IEEE, 2017, pp. 736–741.